Lack of the endosomal SNAREs vti1a and vti1b led to significant impairments in neuronal development

Ajaya J. Kunwar[a,1], Michael Rickmann[a,1], Bianca Backofen[b], Sascha M. Browski[b], Joachim Rosenbusch[a], Susanne Schöning[b], Thomas Fleischmann[a], Kerstin Krieglstein[a,c,2], and Gabriele Fischer von Mollard[b,2]

[a]Department of Neuroanatomy, Center of Anatomy, University of Göttingen, 37075 Göttingen, Germany; [b]Department of Biochemistry III, Bielefeld University, 33615 Bielefeld, Germany; and [c]Freiburg Institute for Advanced Studies, School of Life Sciences (FRIAS) and Department of Molecular Embryology, University of Freiburg, 79104 Freiburg, Germany

Edited by Pietro De Camilli, Yale University and Howard Hughes Medical Institute, New Haven, CT, and approved December 30, 2010 (received for review September 15, 2010)

Fusion between membranes is mediated by specific SNARE complexes. Here we report that fibroblasts survive the absence of the trans-Golgi network/early endosomal SNARE vti1a and the late endosomal SNARE vti1b with intact organelle morphology and minor trafficking defects. Because vti1a and vti1b are the only members of their SNARE subclass and the yeast homolog Vti1p is essential for cell survival, these data suggest that more distantly related SNAREs acquired the ability to function in endosomal traffic during evolution. However, absence of vti1a and vti1b resulted in perinatal lethality. Major axon tracts were missing, reduced in size, or misrouted in *Vti1a*$^{-/-}$ *Vti1b*$^{-/-}$ embryos. Progressive neurodegeneration was observed in most *Vti1a*$^{-/-}$ *Vti1b*$^{-/-}$ peripheral ganglia. Neurons were reduced by more than 95% in *Vti1a*$^{-/-}$ *Vti1b*$^{-/-}$ dorsal root and geniculate ganglia at embryonic day 18.5. These data suggest that special demands for endosomal membrane traffic could not be met in *Vti1a*$^{-/-}$ *Vti1b*$^{-/-}$ neurons. *Vti1a*$^{-/-}$ and *Vti1b*$^{-/-}$ single deficient mice were viable without these neuronal defects, indicating that they can substitute for each other in these processes.

endosome | neurite outgrowth | neuronal survival

In eukaryotic cells, membrane-enclosed organelles communicate by vesicular traffic. Membrane trafficking pathways are classified into a biosynthetic/exocytotic limb and an endocytotic/degradative limb that originates at the plasma membrane and leads via endosomes to lysosomes (1). Evolutionarily conserved trafficking steps are adapted to generate specialized membrane compartments, such as axons and dendrites in neurons. Each step involves formation of transport vesicles by budding, transport of vesicles to their destination, attachment, and subsequent fusion with the target membrane and is carried out by members of protein families conserved between unicellular eukaryotes and man. In vesicle docking and fusion these families include rab GTPases, Sec1/Munc18-like proteins, and SNAREs (2).

SNAREs catalyze membrane fusion. They are membrane-anchored proteins that usually contain a C-terminal transmembrane domain, an adjacent SNARE motif, and an N-terminal domain (2). Before fusion, the SNARE motifs of SNAREs residing in membranes destined to fuse assemble into a four-helix bundle. Each helix within the four-helix bundle is contributed by a different SNARE motif. Sequence analysis has shown that SNARE motifs are divided into four subgroups: Qa-, Qb-, Qc-, and R-SNAREs (2). The QabcR composition of SNARE complexes is universal, indicating that the diversification of SNAREs into four subfamilies occurred at the basis of eukaryotic evolution. Different intracellular fusion reactions involve SNARE complexes of different composition. Many SNAREs operate in more than one fusion event, sometimes involving different SNARE partners. Conversely, single fusion events may accept an alternative SNARE as substitute. Bioinformatic classification of SNAREs resulted in 20 subgroups that represent the SNARE equipment of the ur-eukaryotic cell and that are associated with fusion events at the endoplasmic reticulum, Golgi, trans-Golgi network (TGN), plasma membrane, and endo-lysosomal system (3, 4). According to this classification, at least one member of each subgroup is required for membrane traffic in every eukaryotic cell.

In yeast, Vti1p is the only SNARE of the endo-lysosomal Qb.IIIb SNARE subclass (3). Vti1p is essential, showing that it cannot be substituted by a Qb-SNARE of another subgroup. It participates in four SNARE complexes in separate steps of endo-lysosomal trafficking (5, 6). In mammals, the Qb.IIIb subgroup is represented by vti1a and vti1b (4). They share only 30% of their amino acids without other related SNAREs (7). In vitro experiments revealed that vti1a and vti1b have functionally diversified. Vti1a forms complexes with the SNAREs syntaxin16 or syntaxin13 (Qa), syntaxin6 (Qc), and VAMP4 (R), which function in fusion of early endosomes and in retrograde transport from endosomes to the TGN (8–10). Vti1b functions in fusion of late endosomes, involving syntaxin7 (Qa), syntaxin8 (Qc), and VAMP8/endobrevin (9). Vti1b, syntaxin7, and syntaxin8 mediate transport from late endosomes to lysosomes in vitro with VAMP7/TI-VAMP (11, 12). These differences are reflected by distinct but overlapping distributions. Vti1a is localized predominantly in the TGN, vti1b in late endosomes (13).

Previously, we created vti1b-deficient mice (14). They were viable and fertile, suggesting that vti1a is capable of substituting vti1b. We have now created *Vti1a*$^{-/-}$ mice, and they are also viable. Surprisingly, *Vti1a*$^{-/-}$ *Vti1b*$^{-/-}$ mice survived until birth, and endo-lysosomal trafficking in double-knockout (DKO) fibroblasts is largely normal. However, these mice displayed widespread defects in major axon tracts and massive neurodegeneration not seen in either single KO. Thus, vti1a and vti1b as the only SNAREs of their subclass are dispensable for maintaining membrane traffic at the basal level. Subtle defects at the single-cell level may synergize to impair the development of neurons, which relies on high-performance trafficking to build enormously expanded membrane systems.

Results

Targeted Disruption of *Vti1a* and Generation of *Vti1a*$^{-/-}$ *Vti1b*$^{-/-}$ Embryos. The gene for vti1a was disrupted by insertion of a neomycin resistance gene into exon 6 (Fig. S1). Vti1a-deficient (*Vti1a*$^{-/-}$) mice were viable and fertile even though vti1a protein was absent, including vti1a-β encoded by a brain-specific splice variant (15; Fig. 1*A*). *Vti1a*$^{-/-}$ and *Vti1b*$^{-/-}$ mice were crossed to

Author contributions: M.R., K.K., and G.F.v.M. designed research; A.J.K., M.R., B.B., S.M.B., J.R., S.S., and T.F. performed research; A.J.K., M.R., B.B., S.M.B., K.K., and G.F.v.M. analyzed data; and A.J.K., M.R., K.K., and G.F.v.M. wrote the paper.

The authors declare no conflict of interest.

This article is a PNAS Direct Submission.

[1]A.J.K. and M.R. contributed equally to this work.

[2]To whom correspondence may be addressed. E-mail: kerstin.krieglstein@anat.uni-freiburg.de or gabriele.mollard@uni-bielefeld.de.

This article contains supporting information online at www.pnas.org/lookup/suppl/doi:10.1073/pnas.1013891108/-/DCSupplemental.

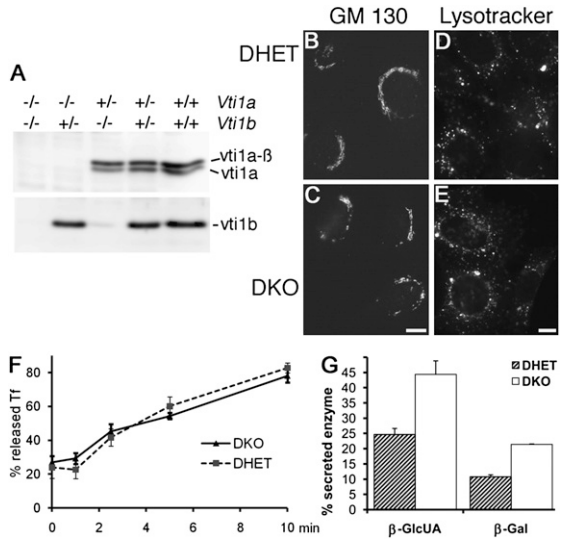

Fig. 1. Intact organelle morphology but increased secretion of lysosomal enzymes in *Vti1a*$^{-/-}$ *Vti1b*$^{-/-}$ fibroblasts. (*A*) Targeted disruption of the *Vti1a* or *Vti1b* locus results in absence of these proteins detected with antibodies in E18.5 brain lysates. Immortalized *Vti1a*$^{-/-}$ *Vti1b*$^{-/-}$ (DKO) and *Vti1a*$^{+/-}$ *Vti1b*$^{+/-}$ (DHET) fibroblasts were stained for the Golgi marker GM130 (*B* and *C*) and lysotracker as marker for late endosomes and lysosomes (*D* and *E*). (*F*) DKO and DHET fibroblasts released transferrin with similar kinetics. Cells were allowed to release endocytosed biotinylated transferrin. Transferrin in medium and cells was quantified after SDS/PAGE with streptavidin-HRP (±SEM, $n = 4$). (*G*) DKO fibroblasts secreted more lysosomal β-glucuronidase (β-GlcUA, ±SEM, $P = 0.02$, unpaired Student's t test, $n = 3$) and β-galactosidase ($n = 2$) than DHET cells. Activity was determined in medium and cells.

determine whether both proteins are redundant. *Vti1a*$^{+/-}$ *Vti1b*$^{-/-}$ and *Vti1a*$^{-/-}$ *Vti1b*$^{+/-}$ mice survived and were fertile. Surprisingly, *Vti1a*$^{-/-}$ *Vti1b*$^{-/-}$ (DKO) embryos completed their development and died at birth. This indicates that membrane traffic is sufficiently functional for maintaining cell function and differentiation during development. To assess endo-lysosomal transport, we immortalized fibroblasts isolated from E12.5 DKO and double heterozygous (DHET) embryos. First, we studied organelle morphology using markers including GM130 for Golgi (Fig. 1 *B* and *C* and Fig. S2), LAMP2, and lysotracker for acidic late endosomes and lysosomes (Fig. 1 *D* and *E* and Fig. S2) and for TGN and early endosomes (Fig. S2). However, no significant differences were observed in the staining patterns between DKO and DHET fibroblasts. Together, these findings indicate that the overall architecture of the organelles constituting the secretory and endo-lysosomal pathway is not significantly affected by the lack of both vti1 proteins.

Next we investigated endo-lysosomal trafficking pathways. We analyzed uptake and release of transferrin that binds to transferrin receptors. The complex is endocytosed by clathrin-mediated endocytosis and travels through endosomes before being recycled to the plasma membrane, where transferrin is released. Endocytosis of fluorescent transferrin was similar in DHET and DKO cells (Fig. S3*A*). To examine effects on recycling rates, we monitored release kinetics of transferrin. Endocytosed biotinylated transferrin was released with similar kinetics into the medium in both fibroblasts (Fig. 1*F*). We probed for trafficking routes directed toward lysosomes. Most newly synthesized soluble lysosomal enzymes are recognized in the TGN by mannose-6-phosphate receptors (MPR) and transported by clathrin-coated vesicles to late endosomes. Receptors recycle to the TGN, whereas cargo continues to lysosomes. In the absence of MPRs lysosomal enzymes follow the default pathway from the TGN to the plasma membrane for secretion (16). Interference with vti1a function results in reduced transport of MPRs from endosomes to the TGN in vitro (10, 17) and in increased secretion of lysosomal enzymes (17). We found that DKO fibroblasts secreted almost twice as much lysosomal β-glucuronidase and β-galactosidase normalized to total enzyme content (Fig. 1*G*). We did not observe a significant change in localization of MPR-46, suggesting that a reduced transport capacity in DKO cells is not reflected by a change in steady-state distributions of the receptors (Fig. S2).

Defects in trafficking between TGN and late endosomes prompted us to investigate trafficking to lysosomes. We monitored the fate of EGF after internalization. EGF is endocytosed after binding to EGF receptors. After reaching early endosomes, the complex is transported via late endosomes to lysosomes for degradation (18). Fibroblasts were incubated with fluorescent EGF, resulting in a depletion of EGF receptors from the plasma membrane and subsequently a reduction of internalized EGF due to degradation in lysosomes. No difference was detectable between DKO and DHET cells (Fig. S3*B*). We investigated whether fusion of autophagosomes with lysosomes is affected. Autophagosomes are induced by starvation for amino acids. After enclosure of cytoplasm with a double membrane, autophagosomes fuse with lysosomes, followed by degradation of autophagosomal content (19). Autophagy was determined by degradation of radioactive cellular proteins and was comparable for DKO and DHET fibroblasts under starvation conditions (Fig. S3*C*).

Taken together, our results show that trafficking routes between the plasma membrane, early and late endosomes, and lysosomes do not display overt defects in the absence of vti1a and vti1b, with the only observable phenotype being transport of lysosomal enzymes. Why do DKO mice die at birth? Because DKO brains were smaller, we performed a detailed analysis of brain development.

Impaired Axon Growth in the Absence of vti1a and vti1b. Severe defects were detectable in the development of central and peripheral nervous system in DKO compared with wild-type, DHET, *Vti1a*$^{+/-}$ *Vti1b*$^{-/-}$, and *Vti1a*$^{-/-}$ *Vti1b*$^{+/-}$ embryos. Embryonic day (E) 18.5 DKO brains were smaller and showed wider ventricles (Fig. 2*B*, asterisk, and Fig. S4*S*) compared with DHET littermates (Fig. 2*A*, asterisk, and Fig. S4*R*). Ventricular size was similar at E14.5 (Fig. 3 *G* and *H*), suggesting that brain growth and differentiation may be primarily affected in DKO. Neurons generate extensions, dendrites, and axons. In DKO mice, major projection tracts and commissures were absent or reduced in size. The anterior commissure, a bundle of axonal fibers that runs transversely to connect ventral and anterior parts of cortical hemispheres, was absent in DKO (Fig. 2*B* in coronal, Fig. 2*D* in sagittal views, yellow arrows). The hippocampal commissure (Fig. 2*B*, black arrow) and the fibers of fornix (Fig. 2*F*, arrow) are missing in E18.5 DKO mice. The corpus callosum was greatly reduced in anteroposterior extent (Fig. 2*D*, bracket) and thickness (Fig. 2*F*, bracket) compared with DHET (Fig. 2 *A*, *C*, and *E*). The optic tract and chiasma were diminished in DKO (Fig. 2*H*, arrow). Commissural fibers connect the two hemispheres and are involved in coordination of highly processed information across hemispheres required for auditory and visual system, memory, learning, and emotional behavior. All commissural fibers cross the midline. Guiding axons to cross the midline is a task of midline glia, specifically in development of the corpus callosum (20). Using GFAP and nestin immunocytochemistry no aberration in development of midline glia could be detected, suggesting that the defects are not due to glial impairments. The data strongly argue for impaired axon growth as the basis of the lack of projections and several classes of commissural fibers.

An unusual bundle of fibers was found on the lateral side of DKO striatum (Fig. 3 *A* and *B*, yellow arrows). To identify the origin of these fibers neuronal tract tracing was applied. Anterograde DiI-tracing revealed that these fiber bundles contained corticostriatal fibers (Fig. 3 *C* and *D*, yellow arrows) but not

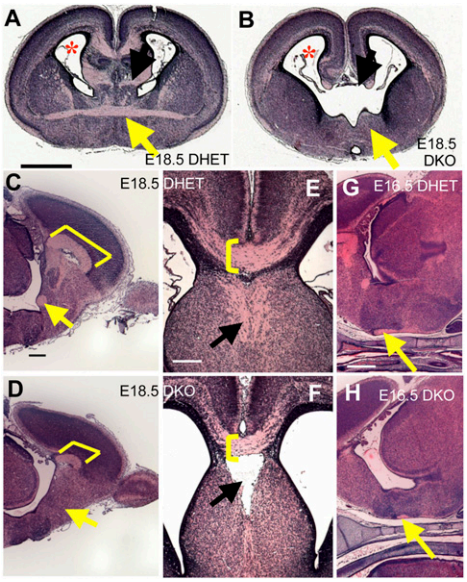

Fig. 2. General phenotype of DKO mice. At E18.5 the size of the DKO brain is reduced, lateral ventricles (*B*, asterisk) are enlarged, and the hippocampal commissure (*B*, black arrow) and anterior commissure are missing (*B*, yellow arrow) compared with DHET (*A*) in H&E staining. Absence of the anterior commissure in DKO in sagittal view (*D*, arrow) in contrast to DHET (*C*). The anteroposterior extent (*D*, bracket) and thickness (*F*, bracket) of the corpus callosum is reduced in DKO compared with DHET (*C* and *E*). Missing fibers of fornix leave a gap in DKO (*F*, arrow). In a sagittal view of E16.5 DKO mice the optic chiasma is smaller (*H*, arrow) than in DHET (*G*). (Scale bars, 1,000 μm in *A* and *B*, 500 μm in *G* and *H*, 250 μm in *C* and *D*, 100 μm in *E* and *F*.)

thalamostriatal because fibers were labeled by DiI application to cortex but not to thalamus (Fig. 3 *E* and *F*, yellow arrows). The majority of fibers in the medial part of the striatum at E18.5 were missing (Fig. 3 *B*, *D*, and *F*, blue arrows). These fiber bundles contain DiI-labeled corticostriatal (Fig. 3*C*, blue arrows) and thalamocortical (Fig. 3*E*, blue arrows) axons. Thalamocortical axons (TCA; connecting thalamus and cortex) are major projection fibers, which are defective in DKO mice. So far, the data suggest that major projection fibers are lacking, whereas others are misrouted. To identify all axons present, neurofilament labeling was performed. By E14.5, neurofilament-labeled thalamocortical axons just reached the cortex in DHET (Fig. 3*G*, arrow), in DKO they did not cross the pallio-subpallial border (Fig. 3*H*, arrow). By E18.5, TCA reached most of the cortex in DHET (Fig. S4*R*, arrow); in DKO they stopped halfway and stayed within the internal capsule region (Fig. S4*S*). These data show that axon growth and possibly axon guidance at the level of the pallio-subpalladial border is impaired in TCA. We used DiI to selectively label TCA and corticofugal axons separately. DiI-labeled DKO thalamocortical axons did not reach the cortex and stopped halfway (Fig. 3 *I* and *J*), confirming the neurofilament labeling. DiI paste was applied to the cortex to label corticofugal axons. Only few fibers left the cortex in E16.5 DKO (Fig. 3*L*, arrow), whereas in controls (here *Vti1a*$^{+/-}$ *Vti1b*$^{-/-}$) a thick bundle of fibers was labeled (Fig. 3*K*, arrow). The data presented document that numerous fiber tracts within the CNS are missing, reduced in size, or misrouted, indicating impaired axon guidance and/or axon growth.

Progressive Degeneration of the Peripheral Nervous System. Ganglia contain accumulations of neuronal cell bodies in the peripheral nervous system, which survive because of target-derived neurotrophins. In DKO embryos peripheral ganglia show different degrees of neurodegeneration. Trigeminal, nodose, petrosal, geniculate, and dorsal root ganglia (DRG) show severe progressive neurodegeneration, superior cervical ganglia (SCG) moderate, whereas vestibular and cochlear ganglia were least affected (Fig. 4, Fig. S4, and Table S1). Reduction in size of DKO trigeminal ganglia started at E12.5 (Fig. 4 *A* and *B*). At E14.5 they were shrunk by 86.3% (Fig. 4 *C* and *D*) and at E18.5 by 97.8% (Fig. 4 *E* and *F*). Neuronal death in DKO trigeminal ganglia occurred via a caspase-mediated pathway. Significant numbers of activated caspase-3–positive apoptotic neurons were seen in DKO (Fig. 4 *G* and *H* and Fig. S4). In E14.5 DKO DRG, the reduction in cell number was 84.3% (Fig. 4 *K* and *L*). By E18.5, DRGs had almost disappeared (Fig. 4 *M* and *N*). Neurodegeneration in vestibular (Fig. 4 *I* and *J* and Fig. S4) and cochlear ganglia (Fig. S4) was the lowest. At E18.5, their cell numbers were reduced by 14.9% and 26%, respectively (Table S1). Correspondingly, low numbers of apoptotic neurons were detected (Fig. S4). Both vti1a and vti1b

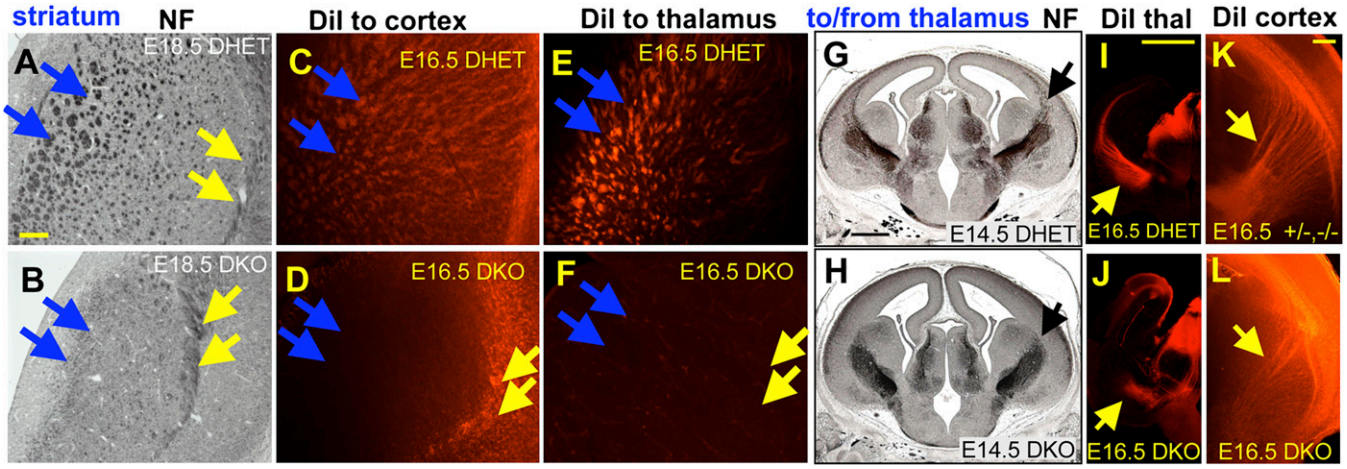

Fig. 3. Cortical fiber tracts. (*A*–*F*) To striatum. Neurofilament-labeled (NF, *A* and *B*) tissue showed bundle of fibers at the lateral side of the striatum in DKO (*B*, yellow arrows) but not DHET (*A*). These bundles contain corticostriatal axons as traced with DiI (*D*, yellow arrows) but no thalamostriatal fibers (*F*, yellow arrows). The fiber bundles in the medial striatum of DHET (*A*, blue arrows) with corticostriatal (*C*, blue arrows) and thalamocortical (*E*, blue arrows) axons were absent in DKO (*B*, *D*, and *F*). (*G*–*L*) To/from the thalamus. At E14.5 TCA cannot cross the pallio-subpallial border (arrow in *H*) in DKO compared with DHET (*G*). This is confirmed by DiI to thalami at E16.5 in DKO (*J*, arrow) and DHET (*I*). DiI-labeled corticofugal fibers are fewer in E16.5 DKO (*L*, arrow) than in *Vti1a*$^{+/-}$ *Vti1b*$^{-/-}$ controls (*K*). (Scale bars, 100 μm in *A*–*F*, 200 μm in *K* and *L*, 500 μm in *G* and *H*, 1,000 μm *I* and *J*.)

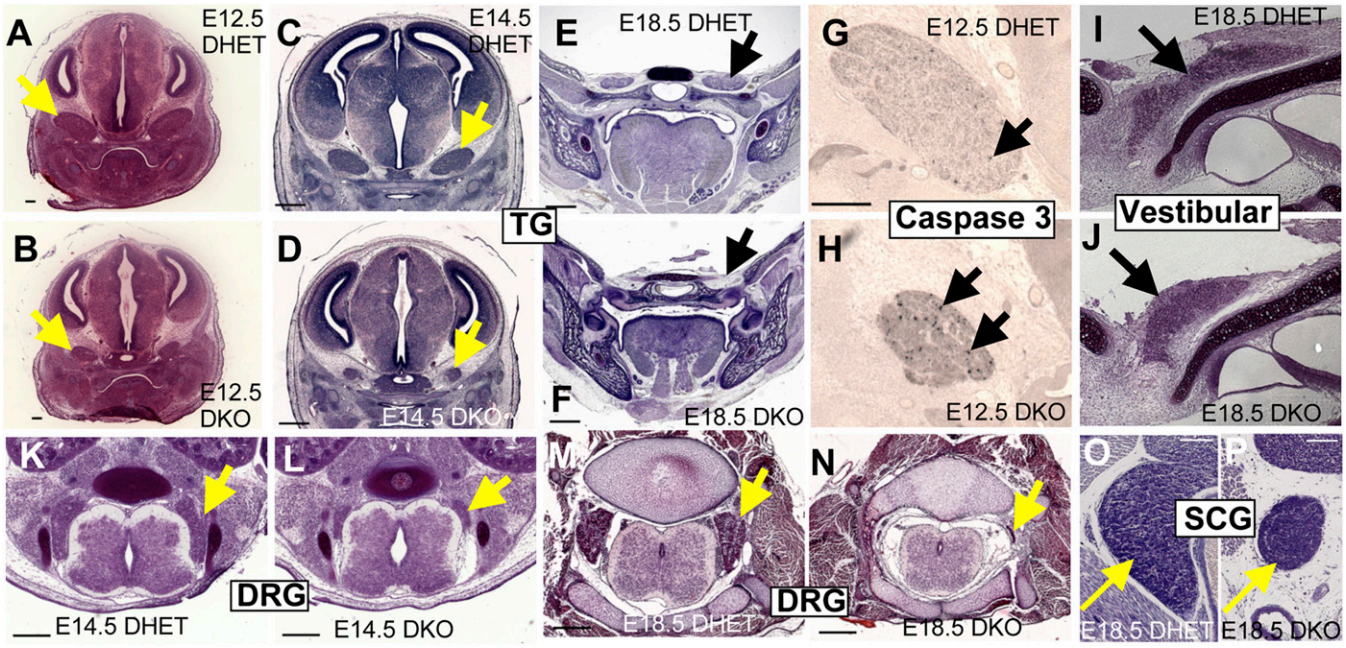

Fig. 4. Different levels of neurodegeneration in peripheral ganglia. Trigeminal ganglia (TG, arrows in *A–H*) and DRG (arrows in *K–N*) are severely degenerated. Vestibular ganglia (*I* and *J*) are least affected. SCG (*O* and *P*) are intermediately reduced. Neurodegeneration in DKO trigeminal ganglion has started at E12.5 (*A*), and activated caspase-3–positive apoptotic neurons are increased (*H*) compared with DHET (*G*). (Scale bars, 250 μm in *A* and *B*, 200 μm *G* and *H*, 500 μm *C–F* and *K–N*, 100 μm *I*, *J*, *O*, and *P*.)

mRNA and protein were present in vestibular ganglia (Fig. S5), excluding lack of vti1a and vti1b expression as cause for low neurodegeneration in these ganglia. SCG showed intermediate degeneration, similar to spinal lumbar motor neurons (L2 level, Table S1). SCG were not affected at E14.5 (Fig. S4) but showed 54% reduction at E18.5 (Fig. 4 *O* and *P*).

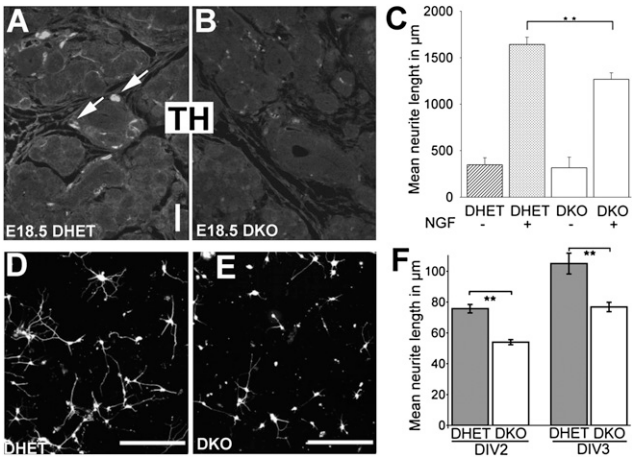

Fig. 5. Defects in neurites. Tyrosine hydroxylase (TH)-positive fibers are absent in the DKO mandibular gland at E18.5 (*A* and *B*), which is a target organ for superior cervical ganglion. (Scale bar, 50 μm.) (*C*) DRG from E12.5 littermates were cultivated in the absence or presence of NGF. NGF stimulated neurite outgrowth from DHET and DKO explants, but neurite length was significantly shorter in DKO (mean ± SEM, $^{**}P = 0.003$, unpaired Student's *t* test, $n = 9$ DKO, $n = 8$ DHET). (*D* and *E*) Fewer hippocampal neurons can be cultivated from E18.5 DKO, and their neurites are less developed after 2 days in vitro (DIV). Neurons were stained for βIII tubulin. (Scale bars, 250 μm.) (*F*) Hippocampal neurite length was shorter in DKO (mean ± SEM, $^{**}P < 0.001$ unpaired Student's *t* test, $n = 8$ DKO, $n = 5$ DHET).

To test whether the degeneration of the peripheral nervous system may be due to lack of target innervation, tyrosine hydroxylase immunostaining of SCG axons in the mandibular gland was performed. In E18.5 DKO mandibular gland, no tyrosine hydroxylase-positive fibers were detected (Fig. 5*B*); DHET showed them at normal density (Fig. 5*A*). These results suggest that SCG neurons did not reach their target and may have died owing to lack of neurotrophic support. The results so far indicate an impairment of axon outgrowth that may be caused by an insufficient rate of plasma membrane insertion. Because most peripheral neurons depend on target-derived neurotrophic factors for survival (21), neurons lacking vti1a and vti1b may become unresponsive to these survival factors. Neurotrophin signaling requires endocytosis and retrograde transport of endosomes, as seen for target-derived NGF in DRG neurons (22). To test for neurotrophin responsiveness and for induced neurite growth, DRG explants (E12.5) were grown in the presence or absence of NGF. E12.5 DKO DRGs were already smaller than DHET DRGs. NGF induced neurite outgrowth in both DKO and DHET explants (Fig. 5*C*). However, the longest neurites from NGF-treated DKO explants were significantly shorter compared with DHET. Hippocampal neurons were cultured as a model system for neurite outgrowth in neurons of the CNS. Fewer neurons could be cultivated from E18.5 DKO hippocampi compared with DHET littermates, and they differed in their morphology (Fig. 5 *D* and *E*). Sixty-eight percent of DKO neurons formed neurites after 2 days in culture, which was significantly lower than DHET (87%; Fig. S6*A*). DKO neurites were significantly shorter (Fig. 5*F*). The vti1b partner VAMP7 is involved in neurite outgrowth in a pathway activated by laminin (23, 24). Therefore, neurons were cultivated on laminin or poly-L-lysine, which allows for neurite outgrowth by a different pathway. Neurite development was similar on both substrates independent of the genotype (Fig. S6). Investigating organelle morphology immunofluorescence for GM130, TGN38, MPR46, LAMP1, and synaptobrevin did not reveal obvious differences between DKO and DHET hippocampal neurons (Fig. S7). Distribution of the adhesion molecule L1

was similar in DKO neurons (Fig. S7). L1 is concentrated in axons and travels through a VAMP7 compartment (25). Vti1a did not colocalize with L1. Few organelles were detected that contained both vti1b and L1 (Fig. S8).

Together, these data suggest that axon growth is limited and may occur only at reduced speed in DKO neurons. Impaired axonal growth may be the reason for misrouted axons, because axon guidance is a spatiotemporally regulated process. If axons have not entered the right place at the right time, guidance cues and growth promoting signals will not be sensed, which will lead to misrouted axon projections followed by impaired growth promotion and neuron survival.

Discussion

We report that both vti1a and vti1b, the only mammalian Qb-SNAREs of the endo-lysosomal subclass, are not required for maintaining basic membrane traffic. However, absence of vti1a and vti1b resulted in perinatal lethality in mice, which could be attributed to defects in axonal growth, resulting in missing or misguided axon bundles in the CNS and apoptotic degeneration of neurons in peripheral ganglia. Trafficking defects that other cells tolerate become limiting in neurons.

Surprisingly, DKO embryos develop until E18.5, indicating that most cells survive without vti1a and vti1b, the only members of the endo-lysosomal Qb.IIIb SNARE subclass (4). Yeast cells are nonviable without their only Qb.IIIb SNARE Vti1p (6). A SNARE of another subclass must compensate for the loss of vti1a and vti1b. There are only three other Qb SNAREs in mouse. They function in endoplasmic reticulum and Golgi traffic, each with a yeast ortholog. Because the yeast orthologs are unable to replace Vti1p, it is unlikely that these mammalian Qb SNAREs substitute for vti1a and vti1b. Four mammalian SNAREs contribute Qb and Qc helices: SNAP-23 acts in fusion with the plasma membrane (2). SNAP-25 cannot compensate in most cells because it is specifically expressed in neuroendocrine cells. Likely candidates for compensation are SNAP-29 and SNAP-47 (26, 27), which localize to internal membranes and diverge more from the yeast exocytic Sec9p than SNAP-23. SNAP-29 functions in endocytic recycling (28). The expanding SNARE repertoire provides one mechanism for redundancies. Our data suggest additional redundancies. A SNARE with the ability to operate in endo-lysosomal traffic must have evolved from a SNARE with a function in a different pathway.

Fewer endosomal trafficking steps were affected in DKO fibroblasts than expected (Fig. S9*A*). Autophagocytosis was impaired by vti1b siRNA (29). Autophagocytosis was not delayed in DKO fibroblasts, suggesting an adaptation to the permanent absence of these SNAREs. Fusion with late endosomes and lysosomes is sensitive to antibodies against vti1b (9). In vitro vti1a functions in homotypic fusion of early endosomes (8, 9). These defects were not observed in DKO fibroblasts, indicating that antibodies and expression of soluble SNAREs may also interfere with compensatory SNAREs. DKO fibroblasts had increased secretion of lysosomal enzymes. This is probably due to defects in cycling of MPR between TGN and late endosomes (Fig. S9*A*), even though we did not observe differences in MPR steady-state distribution. Return of MPR to the TGN depends on vti1a and its partner syntaxin16 in vitro (10, 17, 30).

The phenotypes observed in DKO neurons may be due to impaired axonal outgrowth, axonal guidance, or retrograde signaling because endosomal membrane traffic has been implicated in these processes. In axonal outgrowth the plasma membrane of growth cones is expanded by fusion of membranes derived from different compartments (Fig. S9*B*): directly from the TGN, by transcytosis (e.g., of L1) via early endosomes, or from lysosomes (31–33). Endocytosis is required for growth cone dynamics and thus for neurite outgrowth (34, 35). Neurite outgrowth in culture is sensitive to interference with SNARE partners of vti1a, syntaxin13 (36), syntaxin6 (37), and syntaxin16 (38). VAMP7 is involved in neurite outgrowth, especially on laminin (23, 24). DKO neurite outgrowth was similar on laminin and poly-L-lysine. This may be due to compensation by the VAMP2-dependent pathway, which was blocked by Gupton and Gertler (23) but which we did not inhibit. On the other hand, vti1b probably does not participate directly in VAMP7-dependent exocytosis because VAMP7 interacts with SNAP23 and syntaxin4 in lysosomal exocytosis (39). Our data indicate that neurite outgrowth is impaired in DKO brains. Growth cones are guided by attractive or repulsive signaling molecules. Secretion of the guidance molecule Wnt requires endosomal recycling of its binding protein Wls/Evi (40), linking it to endosomal transport. Endocytosis also occurs during growth cone collapse in response to a repulsive signal (41).

Most importantly, endosomes are essential for neuronal survival in target-derived neurotrophin retrograde signaling (Fig. S9*B*). Neurotrophins bound to Trk receptors are endocytosed into signaling endosomes, transported via axons to cell bodies, and activate specific pathways (22, 42). In several DKO ganglia, cell loss was as dramatic as in ganglia triple deficient for the neurotrophins NT-3, BDNF, and NT-4 (21). DKO DRG neurons were able to react to NGF in vitro. Thus, neurotrophin signaling from the plasma membrane was functional. Cell numbers in cochlear and vestibular ganglia were only slightly reduced in DKO, even though they require NT-3 or BDNF (43). Axons of cochlear and vestibular neurons are shorter than axons of strongly affected neurons and may not be as dependent on retrograde signaling via endosomes. Alternatively, they may express more compensating SNAREs. Timing of cell loss correlated with neurite outgrowth and neurotrophin dependency in DKO trigeminal ganglia. Smaller trigeminal ganglia with apoptotic cells were observed at E12.5, with progressive cell loss at E14.5 and E18.5. In $TrkB^{-/-}$ trigeminal ganglia apoptosis peaks at E11 and E12, in $TrkA^{-/-}$ at E13 and E14 (44). Delays or defects in neurite outgrowth as observed for DKO SCG neurons may contribute to the reduction of neurons. E12.5 DKO DRGs were already smaller, indicating that the onset of the phenotype is too early for neurite outgrowth as only cause. Cell loss in DRGs starts at E11 in the absence of local NT-3 before target innervation between E13 and E16 (45).

Our data clearly show that vti1a and vti1b can substitute for each other in the nervous system because DKO mice display severe neuronal phenotypes, whereas mice survive in the absence of vti1a or vti1b without overt phenotypes. These results stress the importance of endosomal trafficking for neuronal survival, axon growth, and pathfinding. The degree of redundancy between endosomal SNAREs was higher than expected. Defects became detectable only in situations of high demand for endosomal trafficking or specialized endosomal function.

Methods

Embryonic Fibroblasts. Immortalized fibroblasts (mouse embryonic fibroblasts, MEFs) from E12.5 littermates were incubated with 50 nM Lysotracker Red DND-99 (Invitrogen) in DMEM + 1% BSA, washed, and fixed in 4% paraformaldehyde (PFA) in PBS. Transferrin recycling was performed as previously described (46). After starvation, MEFs were incubated with 50 μg/mL biotinylated transferrin in DMEM, 1% BSA for 30 min at 37 °C, washed with DMEM, stripped with 150 mM NaCl, 10 mM acetic acid (pH 3.5) and washed with DMEM. Cells were chased with 0.5 mg/mL holo-transferrin and 0.1 mM deferoxamine mesylate in DMEM for 0–10 min. Cell and medium samples were separated by SDS/PAGE, incubated with streptavidin-HRP, and quantified by ECL. The percentage of released transferrin was determined from two blots and two different exposure times for each experiment. MEFs were washed and incubated with DMEM, 1% BSA for 20 h. Supernatant and cell extracts were assayed for β-glucuronidase and β-galactosidase using 4-methylumbelliferyl substrates (16).

Morphological Studies and DiI Labeling. Embryos (E12.5–E16.5) were immersion-fixed in Bouin's fixative; E18.5 embryos were transcardially perfused with

4% PFA. Brains, bodies, and skulls were postfixed in Bouin's fixative for 5 to 6 h, washed with ethanol, and embedded in paraffin. Serial sections of 8–10 μm were mounted on albumin-glycerin–coated slides. For thalamocortical and thalamostriatal axons, E16.5 heads were fixed in 4% PFA overnight after exposure of the skull. Brains were removed and fixed for another day. DiI paste (Invitrogen) was applied to both sides of the dorsal thalamus (a small vertical slit had been made on either side). DiI paste was fixed by drops of 2% agarose. Brains were left in fresh PFA for 3 wk at 37 °C, immersed in 30% sucrose, and cut by vibrotome into 100- to 120-μm sections. DiI paste was applied to most parts of the frontal and parietal cortex to label the corticofugal and corticostriatal axons.

Neurite Outgrowth in DRG Explant Cultures. E12.5 DRG were collected in cold Ham's F12. The ganglia were resuspended in DRG medium, containing F12 DMEM 1:1, N1-Supplement, 100 μg/mL neomycin, 0.25% BSA, 1% L-glutamine, and 1% penicilline/streptomycine. Explant cultures were set up on coverslips coated with poly-L-lysine and laminin. Ganglia were cultivated in 50 μL DRG medium with or without NGF (10 ng/mL) for 16 h. After replacement with 500 μL of the same medium, explants were cultivated for a further 32 h. DRGs were fixed and stained with toluidine blue. Neurite outgrowth was quantified by measuring the 10 longest neurites per ganglion and by calculating the average length for each embryo.

ACKNOWLEDGMENTS. This article is dedicated to the late V. Atlashkin, who generated *Vti1a*$^{-/-}$ mice. We thank C. Wiegand and C. Prange for excellent technical assistance; M. Schindler and H. Riedesel for blastocyst injections; and A. Ziesenis and his team for mouse breeding. This work was funded through Deutsche Forschungsgemeinschaft (DFG) Grants FI583/4-1, Kr1477/11–3, SFB780-B02, and SFB523-B16.

1. Bonifacino JS, Glick BS (2004) The mechanisms of vesicle budding and fusion. *Cell* 116: 153–166.
2. Jahn R, Scheller RH (2006) SNAREs—engines for membrane fusion. *Nat Rev Mol Cell Biol* 7:631–643.
3. Kloepper TH, Kienle CN, Fasshauer D (2007) An elaborate classification of SNARE proteins sheds light on the conservation of the eukaryotic endomembrane system. *Mol Biol Cell* 18:3463–3471.
4. Kloepper TH, Kienle CN, Fasshauer D (2008) SNAREing the basis of multicellularity: Consequences of protein family expansion during evolution. *Mol Biol Evol* 25: 2055–2068.
5. Fischer von Mollard G, Stevens TH (1999) The *Saccharomyces cerevisiae* v-SNARE Vti1p is required for multiple membrane transport pathways to the vacuole. *Mol Biol Cell* 10:1719–1732.
6. von Mollard GF, Nothwehr SF, Stevens TH (1997) The yeast v-SNARE Vti1p mediates two vesicle transport pathways through interactions with the t-SNAREs Sed5p and Pep12p. *J Cell Biol* 137:1511–1524.
7. Fischer von Mollard G, Stevens TH (1998) A human homolog can functionally replace the yeast vesicle-associated SNARE Vti1p in two vesicle transport pathways. *J Biol Chem* 273:2624–2630.
8. Mallard F, et al. (2002) Early/recycling endosomes-to-TGN transport involves two SNARE complexes and a Rab6 isoform. *J Cell Biol* 156:653–664.
9. Antonin W, et al. (2000) A SNARE complex mediating fusion of late endosomes defines conserved properties of SNARE structure and function. *EMBO J* 19:6453–6464.
10. Medigeshi GR, Schu P (2003) Characterization of the in vitro retrograde transport of MPR46. *Traffic* 4:802–811.
11. Martinez-Arca S, et al. (2003) A dual mechanism controlling the localization and function of exocytic v-SNAREs. *Proc Natl Acad Sci USA* 100:9011–9016.
12. Pryor PR, et al. (2004) Combinatorial SNARE complexes with VAMP7 or VAMP8 define different late endocytic fusion events. *EMBO Rep* 5:590–595.
13. Kreykenbohm V, Wenzel D, Antonin W, Atlachkine V, von Mollard GF (2002) The SNAREs vti1a and vti1b have distinct localization and SNARE complex partners. *Eur J Cell Biol* 81:273–280.
14. Atlashkin V, et al. (2003) Deletion of the SNARE vti1b in mice results in the loss of a single SNARE partner, syntaxin 8. *Mol Cell Biol* 23:5198–5207.
15. Antonin W, Riedel D, von Mollard GF (2000) The SNARE Vti1a-beta is localized to small synaptic vesicles and participates in a novel SNARE complex. *J Neurosci* 20: 5724–5732.
16. Kasper D, Dittmer F, von Figura K, Pohlmann R (1996) Neither type of mannose 6-phosphate receptor is sufficient for targeting of lysosomal enzymes along intracellular routes. *J Cell Biol* 134:615–623.
17. Ganley IG, Espinosa E, Pfeffer SR (2008) A syntaxin 10-SNARE complex distinguishes two distinct transport routes from endosomes to the trans-Golgi in human cells. *J Cell Biol* 180:159–172.
18. Sorkin A, Goh LK (2009) Endocytosis and intracellular trafficking of ErbBs. *Exp Cell Res* 315:683–696.
19. Eskelinen EL (2008) New insights into the mechanisms of macroautophagy in mammalian cells. *Int Rev Cell Mol Biol* 266:207–247.
20. Lindwall C, Fothergill T, Richards LJ (2007) Commissure formation in the mammalian forebrain. *Curr Opin Neurobiol* 17:3–14.
21. Liu X, Jaenisch R (2000) Severe peripheral sensory neuron loss and modest motor neuron reduction in mice with combined deficiency of brain-derived neurotrophic factor, neurotrophin 3 and neurotrophin 4/5. *Dev Dyn* 218:94–101.
22. Zweifel LS, Kuruvilla R, Ginty DD (2005) Functions and mechanisms of retrograde neurotrophin signalling. *Nat Rev Neurosci* 6:615–625.
23. Gupton SL, Gertler FB (2010) Integrin signaling switches the cytoskeletal and exocytic machinery that drives neuritogenesis. *Dev Cell* 18:725–736.
24. Martinez-Arca S, Alberts P, Zahraoui A, Louvard D, Galli T (2000) Role of tetanus neurotoxin insensitive vesicle-associated membrane protein (TI-VAMP) in vesicular transport mediating neurite outgrowth. *J Cell Biol* 149:889–900.
25. Alberts P, et al. (2003) Cross talk between tetanus neurotoxin-insensitive vesicle-associated membrane protein-mediated transport and L1-mediated adhesion. *Mol Biol Cell* 14:4207–4220.
26. Holt M, et al. (2006) Identification of SNAP-47, a novel Qbc-SNARE with ubiquitous expression. *J Biol Chem* 281:17076–17083.
27. Steegmaier M, et al. (1998) Three novel proteins of the syntaxin/SNAP-25 family. *J Biol Chem* 273:34171–34179.
28. Rapaport D, Lugassy Y, Sprecher E, Horowitz M (2010) Loss of SNAP29 impairs endocytic recycling and cell motility. *PLoS ONE* 5:e9759.
29. Furuta N, Fujita N, Noda T, Yoshimori T, Amano A (2010) Combinational soluble N-ethylmaleimide-sensitive factor attachment protein receptor proteins VAMP8 and Vti1b mediate fusion of antimicrobial and canonical autophagosomes with lysosomes. *Mol Biol Cell* 21:1001–1010.
30. Amessou M, et al. (2007) Syntaxin 16 and syntaxin 5 are required for efficient retrograde transport of several exogenous and endogenous cargo proteins. *J Cell Sci* 120:1457–1468.
31. Pfenninger KH (2009) Plasma membrane expansion: A neuron's Herculean task. *Nat Rev Neurosci* 10:251–261.
32. Arantes RME, Andrews NW (2006) A role for synaptotagmin VII-regulated exocytosis of lysosomes in neurite outgrowth from primary sympathetic neurons. *J Neurosci* 26: 4630–4637.
33. Sann S, Wang Z, Brown H, Jin Y (2009) Roles of endosomal trafficking in neurite outgrowth and guidance. *Trends Cell Biol* 19:317–324.
34. Mundigl O, et al. (1998) Amphiphysin I antisense oligonucleotides inhibit neurite outgrowth in cultured hippocampal neurons. *J Neurosci* 18:93–103.
35. Bonanomi D, et al. (2008) Identification of a developmentally regulated pathway of membrane retrieval in neuronal growth cones. *J Cell Sci* 121:3757–3769.
36. Hirling H, et al. (2000) Syntaxin 13 is a developmentally regulated SNARE involved in neurite outgrowth and endosomal trafficking. *Eur J Neurosci* 12:1913–1923.
37. Kabayama H, Tokushige N, Takeuchi M, Mikoshiba K (2008) Syntaxin 6 regulates nerve growth factor-dependent neurite outgrowth. *Neurosci Lett* 436:340–344.
38. Chua CEL, Tang BL (2008) Syntaxin 16 is enriched in neuronal dendrites and may have a role in neurite outgrowth. *Mol Membr Biol* 25:35–45.
39. Rao SK, Huynh C, Proux-Gillardeaux V, Galli T, Andrews NW (2004) Identification of SNAREs involved in synaptotagmin VII-regulated lysosomal exocytosis. *J Biol Chem* 279:20471–20479.
40. Belenkaya TY, et al. (2008) The retromer complex influences Wnt secretion by recycling wntless from endosomes to the trans-Golgi network. *Dev Cell* 14:120–131.
41. van Horck FP, Weinl C, Holt CE (2004) Retinal axon guidance: Novel mechanisms for steering. *Curr Opin Neurobiol* 14:61–66.
42. Valdez G, et al. (2005) Pincher-mediated macroendocytosis underlies retrograde signaling by neurotrophin receptors. *J Neurosci* 25:5236–5247.
43. Ernfors P, Van De Water T, Loring J, Jaenisch R (1995) Complementary roles of BDNF and NT-3 in vestibular and auditory development. *Neuron* 14:1153–1164.
44. Piñon LGP, Minichiello L, Klein R, Davies AM (1996) Timing of neuronal death in trkA, trkB and trkC mutant embryos reveals developmental changes in sensory neuron dependence on Trk signalling. *Development* 122:3255–3261.
45. Liebl DJ, Tessarollo L, Palko ME, Parada LF (1997) Absence of sensory neurons before target innervation in brain-derived neurotrophic factor-, neurotrophin 3-, and TrkC-deficient embryonic mice. *J Neurosci* 17:9113–9121.
46. Johnson EE, Overmeyer JH, Gunning WT, Maltese WA (2006) Gene silencing reveals a specific function of hVps34 phosphatidylinositol 3-kinase in late versus early endosomes. *J Cell Sci* 119:1219–1232.